$$\vec{E}_a = \frac{\phi_0}{2K(k_1)}[-\vec{a}_x \mathrm{Re}(dW_1/dZ) + \vec{a}_y \mathrm{Im}(dW_1/dZ)], \quad (5b)$$

$$k_1 = \tanh(\pi a/2h)/\tanh(\pi b/2h), \quad (5c)$$

$$dW_1/dZ = \frac{(\pi/2h)}{\tanh(\pi a/2h)\cosh^2(\pi Z/2h)\sqrt{(1-Z_1^2)(1-k_1^2 Z_1^2)}}, \quad (5d)$$

$$Z_1 = \tanh(\pi Z/2h)/\tanh(\pi a/2h), \quad (5e)$$

$$\vec{E}_b = \frac{\phi_0}{2K(k))}[-\vec{a}_x \mathrm{Re}(dW/dZ) + \vec{a}_y \mathrm{Im}(dW/dZ)] \quad (5f)$$

k and dW/dZ are given in (3b) and (3c), and $k' = \sqrt{1-k^2}$.

III. Results

Our analytical expressions are applied to the supported coplanar waveguide considered in [5] and coplanar strips. The computed field profiles are plotted in Figs. 3 and 4. The results obtained using the point matching method [9] are also given in the figures for comparison. The series expansion including 400 terms is used and the calculated domain is 10 mm. From Fig. 3, one can see that the results for the case $y = -0.3$ mm are not good. However, this is unimportant because only the fields near the electrode gaps are of interest for the practical applications. In Figs. 3 and 4, the results at $y = 0$ obtained by the point matching method are not included because of the serious oscillations. The case $y = -h$ is not calculated since the normal electric field is not continuous. The comparison shows that the proposed analytical expressions give excellent descriptions for the field distributions, even for the case when the coplanar waveguide has a large dielectric difference between the substrate and the supporting material.

IV. Conclusion

In summary, we have derived analytical expressions for calculating the field distributions in two typical supported coplanar lines, including coplanar lines with finitely thick substrate. This method provides an accurate, simple and fast approach to calculating the field distributions in coplanar lines. Calculated results agree well with those obtained using the point matching method. Although only symmetric coplanar waveguide and coplanar strips have been discussed, our method can also be applied to the analysis of other coplanar transmission lines, such as covered supported coplanar waveguide, overlayed coplanar waveguide [5], and modified coplanar stripline [7]. Using the coordinate transformation [11], this method can be extended to analyze the coplanar lines fabricated on anisotropic substrate, which are widely used for integrated optical devices [12]. Hence the present methods are very useful for MMIC and other similar applications where field distributions are essential.

References

[1] C. Veyres and V. Fouad-Hanna, "Extension of the application of conformal mapping techniques to coplanar lines with finite dimensions," *Int. J. Electron.*, vol. 48, pp. 47–56, 1980.

[2] V. Fouad-Hanna and D. Thebault, "Theoretical and experimental investigation of asymmetric coplanar waveguides," *IEEE Trans. Microwave Theory Tech.*, vol. MTT-32, pp. 1649–1651, 1984.

[3] G. Ghione and C. Naldi, "Coplanar waveguides for MMIC applications: effect of upper shielding, conductor backing, finite-extent ground planes, and line-to-line coupling," *IEEE Trans. Microwave Theory Tech.*, vol. MTT-35, pp. 260–267, 1987.

[4] ——, "Analytical formulas for coplanar lines in hybrid and monolithic MIC's," *Electron. Lett.*, vol. 20, pp. 179–181, 1984.

[5] S. S. Bedair and I. Wolff, "Fast, accurate and simple approximate analytic formulas for calculating the parameters of supported coplanar waveguides for (M)MIC's," *IEEE Trans. Microwave Theory Tech.*, vol. 40, pp. 41–48, 1992.

[6] S. S. Gevorgian and I. G. Mironenko, "Asymmetric coplanar-strip transmission lines for MMIC and integrated optic applications," *Electron. Lett.*, vol. 26, pp. 1916–1918, 1990.

[7] J. S. Mclean and T. Itoh, "analysis of a new configuration of coplanar stripline," *IEEE Trans. Microwave Theory Tech.*, vol. MTT-40, pp. 772–774, 1992.

[8] N. H. Zhu, Z. Q. Wang, and W. Lin, "On the accuracy of analytical expressions for calculating the parameters of coplanar strips on a finitely thick substrate," *Microwave Opt. Technol. Lett.*, vol. 7, pp. 160–164, 1995.

[9] D. Marcuse, "Electrostatic field of coplanar lines computed with the point matching method," *IEEE J Quantum Electron.*, vol. QE-25, pp. 939–947, 1989.

[10] T. N. Chang and Y. C. Sze, "Flexibility in the choice of Green's function for the boundary element method," *IEEE Trans. Microwave Theory Tech.*, vol. 42, pp. 1973–1977, 1994.

[11] O. G. Ramer, "Integrated optic electrooptic modulator electrode analysis," *IEEE J. Quantum Electron.*, vol. QE-18, pp. 386–392, 1982.

[12] R. C. Alferness, "Waveguide electrooptic modulators," *IEEE Trans. Microwave Theory Tech.*, vol. MTT-30, pp. 1121–1137, 1982.

Network Representation and Transverse Resonance for Layered Chirowaveguides

Xu Shanjia and Du Kai

***Abstract*— This paper presents an equivalent network method for dispersion analysis of general chirowaveguides. First, wave propagation in each homogeneous layer is represented by two pairs of transmission lines, the matrix wave impedance is defined. Next, the transformation properties of the input impedance are established. It is then demonstrated that the transverse resonance condition involving the previously obtained matrix impedance leads to the dispersion equation for the waveguides. The numerical results show that this network approach is feasible and practicable.**

I. Introduction

In recent years, a number of papers have appeared in the literature [1]–[5] attacking different kinds of chirowaveguides and the guided wave properties in these new waveguides. Creative use of chiral material, especially for integrated circuits, has been envisioned. The multilayered planar chirowaveguides will become the building block and thus is the foundation for analysis of a large class of chiral guided wave structures. In our opinion, the existing methods are not general enough to enable the interested worker in the microwave and millimeter-wave areas to readily solve for the propagation constant

Manuscript received June 10, 1995; revised April 19, 1996.

The authors are with the Department of Electronic Engineering and Information Science, University of Science and Technology of China, Hefei, Anhui, 230027, P. R. China.

Publisher Item Identifier S 0018-9480(96)05638-4.

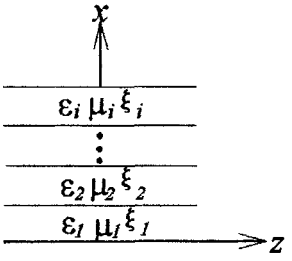

Fig. 1. Multilayered planar chirowaveguide.

and electromagnetic fields in a multilayered planar structure having chiral layers.

The technique of impedance and equivalent network representation is often used to obtain the dispersion characteristics of isotropic waveguides. Based on the experience in treating multimode network problem, we estimated that such a powerful technique can be extended to chiral cases. Indeed, it will be shown in this paper that the network approach provides both insight and a simple solution to the guidance problem of multilayered chirowaveguides.

As a result of the additional coupling mechanisms acting between field components due to the chirality, in the present analysis the wave impedance expands into a 2*2 matrix form, and the coupling between the eigenmodes at the interface of two different chiral layers is represented by an impedance inverter.. In order to use the transverse resonance technique, we also give the necessary impedance transformation relations for different interfaces and boundary conditions. Finally, as an example the surface wave dispersion properties for a two-layer open chirowaveguide are analyzed by the present network method and the effectiveness of the network method is tested.

II. Formulation and Numerical Results

A uniform multilayered planar chiral structure is shown in Fig. 1. The chiral parameters can be zero for anyone of the layers corresponding to the isotropic dielectric. Neither, either, or both of the two semi-infinite regions can be a perfectly electric or magnetic conductor. Such a structure is sufficiently general as a basis for the potential planar chirowaveguides.

In order to establish a network representation for this structure, we first consider the electromagnetic wave propagation property in each homogeneous layer. For $\exp(j\omega t)$ time harmonic fields, one form of the chiral constitutive relations reads

$$\boldsymbol{D} = \epsilon_0(\epsilon \boldsymbol{E} + Z_0 \xi \boldsymbol{H}) \tag{1a}$$

$$\boldsymbol{B} = \mu_0(-Y_0 \xi \boldsymbol{E} + \mu \boldsymbol{H}) \tag{1b}$$

where $\epsilon_0, \mu_0, \epsilon$ and μ have their usual meanings, ξ is the chiral admittance Z_0 and Y_0 are the wave impedance and wave admittance in vacuum. As being used in reference [4], we adopt the normalized distances and a normalized "magnetic field" that are marked with primes

$$x' = k_0 x, \quad y' = k_0 y, \quad z' = k_0 z, \quad \boldsymbol{H}' = Z_0 \boldsymbol{H}. \tag{2}$$

We restrict our discussion for the case in which only plane wave propagation of the form $\exp(-j\beta z')$ will be considered and therefore we have

$$\frac{\partial}{\partial y'} = 0, \quad \nabla' = \frac{1}{k_0}\nabla = \frac{\partial}{\partial x'}\hat{\boldsymbol{e}}_x - j\beta \hat{\boldsymbol{e}}_z. \tag{3}$$

It should be noted that here β is an effective refractive index rather than the longitudinal wavenumber, since z' is a normalized distance. From Maxwell's equations, we can obtain the following matrix

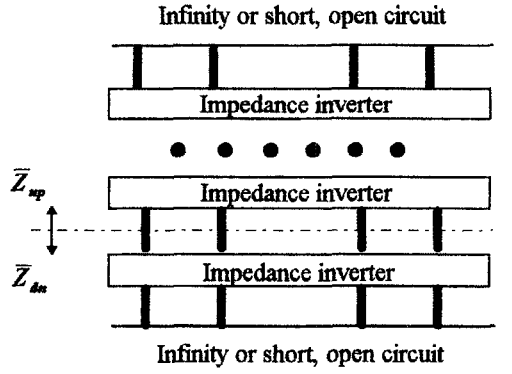

Fig. 2. Transverse equivalent network representation.

equations:

$$\begin{pmatrix} \boldsymbol{E}_x \\ \boldsymbol{H}'_x \end{pmatrix} = \frac{\beta}{\boldsymbol{k}_+\boldsymbol{k}_-}\begin{pmatrix} \xi & \mu \\ -\epsilon & \xi \end{pmatrix}\begin{pmatrix} \boldsymbol{E}_y \\ \boldsymbol{H}'_y \end{pmatrix} \tag{4a}$$

$$\frac{\partial}{\partial \boldsymbol{x}'}\begin{pmatrix} \boldsymbol{E}_y \\ \boldsymbol{H}_y \end{pmatrix} = \begin{pmatrix} \boldsymbol{j}\xi & -\boldsymbol{j}\mu \\ \boldsymbol{j}\epsilon & \boldsymbol{j}\xi \end{pmatrix}\begin{pmatrix} \boldsymbol{E}_x \\ \boldsymbol{H}'_z \end{pmatrix} \equiv \overline{\boldsymbol{A}}\begin{pmatrix} -\boldsymbol{E}_z \\ \boldsymbol{H}'_z \end{pmatrix} \tag{4b}$$

$$\begin{aligned}\frac{\partial}{\partial \boldsymbol{x}'}\begin{pmatrix} \boldsymbol{E}_x \\ \boldsymbol{H}'_z \end{pmatrix} &= \begin{pmatrix} -\boldsymbol{j}\left(1 + \dfrac{\beta^2}{\boldsymbol{k}_+\boldsymbol{k}_-}\right)\xi & \boldsymbol{j}\left(1 - \dfrac{\beta^2}{\boldsymbol{k}_+\boldsymbol{k}_-}\right)\mu \\ -\boldsymbol{j}\left(1 - \dfrac{\beta^2}{\boldsymbol{k}_+\boldsymbol{k}_-}\right)\epsilon & -\boldsymbol{j}\left(1 + \dfrac{\beta^2}{\boldsymbol{k}_+\boldsymbol{k}_-}\right)\xi \end{pmatrix} \\ &\quad \cdot \begin{pmatrix} \boldsymbol{E}_y \\ \boldsymbol{H}'_y \end{pmatrix} \\ &\equiv \overline{\boldsymbol{B}}\begin{pmatrix} -\boldsymbol{E}_y \\ \boldsymbol{H}_y \end{pmatrix}\end{aligned} \tag{4c}$$

in which $\boldsymbol{k}_+\boldsymbol{k}_- = \mu\epsilon + \xi^2, \boldsymbol{k}_+ = \boldsymbol{j}\xi + \sqrt{\mu\epsilon}, \boldsymbol{k}_- = -\boldsymbol{j}\xi + \sqrt{\mu\epsilon}$. Here sign symbol + and − indicate, respectively, the left and right circular polarization. Introducing the transformation matrix $\overline{\boldsymbol{M}}$ so as to diagonalize matrix $\overline{\boldsymbol{A}}$ and $\overline{\boldsymbol{B}}$, and defining the voltage and current column vectors $\boldsymbol{V}$ and $\boldsymbol{I}$ yields

$$\begin{aligned}&\overline{\boldsymbol{M}} = \begin{pmatrix} 1 & 1 \\ \boldsymbol{j}\sqrt{\dfrac{\epsilon}{\mu}} & -\boldsymbol{j}\sqrt{\dfrac{\epsilon}{\mu}} \end{pmatrix}; \quad \boldsymbol{V} = \begin{pmatrix} \boldsymbol{v}_+ \\ \boldsymbol{v}_- \end{pmatrix} = \overline{\boldsymbol{M}}^{-1}\begin{pmatrix} \boldsymbol{E}_y \\ \boldsymbol{H}'_y \end{pmatrix}; \\ &\boldsymbol{I} = \begin{pmatrix} \boldsymbol{i}_+ \\ \boldsymbol{i}_- \end{pmatrix} = \overline{\boldsymbol{M}}^{-1}\begin{pmatrix} \boldsymbol{E}_z \\ \boldsymbol{H}'_z \end{pmatrix}.\end{aligned} \tag{5}$$

Then (4b) and (4c) lead to

$$\begin{aligned}\frac{\partial}{\partial \boldsymbol{x}'}\boldsymbol{v}_+ &= \boldsymbol{k}_+\boldsymbol{i}_+ \\ \frac{\partial}{\partial \boldsymbol{x}'}\boldsymbol{i}_+ &= \left(-\boldsymbol{k}_+ + \frac{\beta^2}{\boldsymbol{k}_+}\right)\boldsymbol{v}_+\end{aligned} \tag{6a}$$

$$\begin{aligned}\frac{\partial}{\partial \boldsymbol{x}'}\boldsymbol{v}_- &= -\boldsymbol{k}_-\boldsymbol{i}_- \\ \frac{\partial}{\partial \boldsymbol{x}'}\boldsymbol{i}_- &= \left(\boldsymbol{k}_- + \frac{\beta^2}{\boldsymbol{k}_-}\right)\boldsymbol{v}_-.\end{aligned} \tag{6b}$$

One can see that (6a) and (6b) have the form of transmission line equations. In fact, the transformation in (5) corresponds to the customary wave splitting technique in attacking chiral problems. The above mathematical manipulation is nothing new; we emphasize here the physical insight gained from (6). These two pairs of transmission line equation constitute the basis of our equivalent network model. One can also see that $\boldsymbol{k}_+$ and $\boldsymbol{k}_-$ are the normalized wave numbers of right circular polarized (RCP) and left circular polarized (LCP) plane waves. Thus, the two pairs of transmission line equations correspond to RCP and LCP plane waves, respectively. Within each homogeneous layer, the propagation constants of the RCP and LCP plane waves are independent. They couple to each other only when

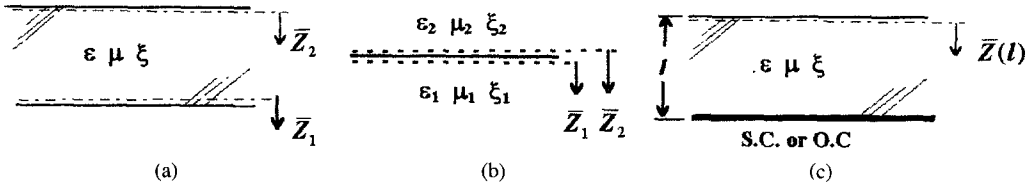

Fig. 3. (a) Impedance transformation within one layer. (b) Impedance transformation at the boundary interface. (c) Input impedance matrix of a layer terminated with open or short circuit.

encountering the discontinuity plane. A transverse equivalent network is shown in Fig. 2, where the coupling process is illustrated by a block.

In order to use the transverse resonance technique to analyze the dispersion of the multilayer chirowaveguides, different kinds of impedance transformation relations are necessary. Without losing generality, we will discuss them in the following three cases:

1) Transformation of input matrix impedance within a homogeneous layer [Fig. 3(a)].

As shown in Fig. 3(a), the input impedance matrices $\overline{Z}_1$ and $\overline{Z}_2$ are defined looking downwards from reference plane 1 and 2. According to the definition of the impedance for the multimode network, we have

$$\boldsymbol{V}_1 = \overline{\boldsymbol{Z}}_1 \boldsymbol{I}_1; \quad \boldsymbol{V}_2 = \overline{\boldsymbol{Z}}_2 \boldsymbol{I}_2 \tag{7}$$

and a matrix eigen-impedance is introduced as

$$\overline{\boldsymbol{Z}}_0 = \begin{pmatrix} \boldsymbol{Z}_{0+} & 0 \\ 0 & \boldsymbol{Z}_0 \end{pmatrix}; \quad \boldsymbol{Z}_{0\pm} = \pm\left[\frac{\boldsymbol{k}_\pm^2}{\beta^2 - \boldsymbol{k}_\pm^2}\right]^{1/2}. \tag{8}$$

Let

$$\overline{\beta}_x = \begin{pmatrix} (\boldsymbol{k}_+^2 - \beta^2)^{1/2} & 0 \\ 0 & (\boldsymbol{k}_-^2 - \beta^2)^{1/2} \end{pmatrix} \tag{9}$$

t is easily found that $\overline{Z}_1$ and $\overline{Z}_2$ obey the following relation

$$\begin{aligned} \overline{\boldsymbol{Z}}_2 = {} & \overline{\boldsymbol{Z}}_1[\cos(\overline{\beta}_x l)\overline{\boldsymbol{Z}}_1 + j\sin(\overline{\beta}_x l)\overline{\boldsymbol{Z}}_0] \\ & \cdot [\cos(\overline{\beta}_x l)\overline{\boldsymbol{Z}}_0 + j\sin(\overline{\beta}_x l)\overline{\boldsymbol{Z}}_1]^{-1}\overline{\boldsymbol{Z}}_0 \end{aligned} \tag{10}$$

where $\cos(\overline{\beta}_x l)$ and $\sin(\overline{\beta}_x l)$ are diagonal matrices, the elements at the nth position in the diagonal matrices are, respectively

$$\begin{aligned} \cos(\overline{\beta}_x l) &= [\delta_{mn}\cos(\overline{\beta}_{xmn} l) \quad \text{and} \\ \sin(\overline{\beta}_x l) &= [\delta_{mn}\sin(\overline{\beta}_{xmn} l)]. \end{aligned}$$

2) Impedance matrix transformation at the interface of two media [Fig. 3(b)].

Referring to Fig. 3(b), the input impedance matrices $\overline{Z}_1$ and $\overline{Z}_2$ are defined just below and above the boundary plane looking toward the interior of material 1

$$\boldsymbol{V}_1 = \overline{\boldsymbol{Z}}_1 \boldsymbol{I}_1; \quad \boldsymbol{V}_2 = \overline{\boldsymbol{Z}}_2 \boldsymbol{I}_2. \tag{11}$$

The boundary conditions read

$$\overline{\boldsymbol{M}}_1 \boldsymbol{V}_1 = \begin{pmatrix} E_y \\ H_y' \end{pmatrix} = \overline{\boldsymbol{M}}_2 \boldsymbol{V}_2; \quad \overline{\boldsymbol{M}}_1 \boldsymbol{I}_1 = \begin{pmatrix} E_x \\ H_z' \end{pmatrix} = \overline{\boldsymbol{M}}_2 \boldsymbol{I}_2 \tag{12}$$

where $\overline{M}_1$ and $\overline{M}_2$ can be obtained by substituting respective material parameters into the definition of $\overline{M}$, and E_y, E_z, H_y', V_1, I_1, etc., are the values of the corresponding components at the boundary. It can be found that

$$\overline{\boldsymbol{Z}}_2 = \overline{\boldsymbol{M}}_2^{-1}\overline{\boldsymbol{M}}_1\overline{\boldsymbol{Z}}_1\overline{\boldsymbol{M}}_1^{-1}\overline{\boldsymbol{M}}_2. \tag{13}$$

3) Input impedance matrix when terminated with open or short circuit [Fig. 3(c)].

In contrast to achiral case, here the input impedance matrix at the surface of a perfect electric or magnetic conductor is not a zero matrix or other constant matrix. This is due to the fact that our "voltages" and "currents" are linear combinations of both electric and magnetic field components. However, the boundary condition of a perfect conductor can be represented by the input impedance matrix looking toward the termination from the interior of the adjacent material. As depicted in Fig. 3(c), we will find a mathematical expression for $\overline{Z}(l)$.

On the surface of an electric (short circuit) or a magnetic (open circuit) conductor, the boundary condition yields for the two components of $\boldsymbol{V}$ and $\boldsymbol{I}$

$$v_+(0) = (-1)^n v_-(0); \quad i_+(0) = (-1)^n i_i(0) \tag{14}$$

where $n =$ corresponds to the short and $n = 2$ to the open circuit. The "voltages" and "currents" on the transmission line can be expressed as

$$\begin{aligned} \begin{pmatrix} \boldsymbol{v}_+(\boldsymbol{l}) \\ \boldsymbol{v}_-(\boldsymbol{l}) \end{pmatrix} = {} & \begin{pmatrix} \cos(\beta_{x+}\boldsymbol{l} & \boldsymbol{j}\boldsymbol{Z}_{0+}\sin(\beta_{x+}\boldsymbol{l}) \\ (-1)^n\cos(\beta_{x-}\boldsymbol{l}) & (-1)^n\boldsymbol{j}\boldsymbol{Z}_{0-}\sin(\beta_{x-}\boldsymbol{l}) \end{pmatrix} \\ & \cdot \begin{pmatrix} \boldsymbol{v}_+(0) \\ \boldsymbol{i}_+(0) \end{pmatrix} \end{aligned} \tag{15a}$$

$$\begin{aligned} \begin{pmatrix} \boldsymbol{i}_+(\boldsymbol{l}) \\ \boldsymbol{i}_i\boldsymbol{l} \end{pmatrix} = {} & \begin{pmatrix} \dfrac{\boldsymbol{j}\sin(\beta_{x+}\boldsymbol{l})}{\boldsymbol{Z}_{0+}} & \cos(\beta_{x+}\boldsymbol{l}) \\ \dfrac{(-1)^n\boldsymbol{j}\sin(\beta_{x-}\boldsymbol{l})}{\boldsymbol{Z}_{0-}} & (-1^n\cos(\beta_{x-}\boldsymbol{l}) \end{pmatrix} \\ & \cdot \begin{pmatrix} \boldsymbol{v}_+(0) \\ \boldsymbol{i}_+(0) \end{pmatrix} \end{aligned} \tag{15b}$$

where

$$\beta_{x+} = \sqrt{k_+^2 - \beta^2}; \quad \beta_{x-} = \sqrt{k_-^2 - \beta^2},$$

Then we have

$$\begin{aligned} \overline{\boldsymbol{Z}}(l) = {} & \begin{pmatrix} \cos(\beta_{x+}l) & jZ_{0+}\sin(\beta_{x+}l) \\ (-1)^n\cos(\beta_{x-}l) & (-1)^n jZ_{0-}\sin(\beta_{x-}l) \end{pmatrix} \\ & \cdot \begin{pmatrix} \dfrac{j\sin(\beta_{x+}l)}{Z_{0+}} & \cos(\beta_{x+}l) \\ \dfrac{(-1)^n j\sin(\beta(\beta_{x-}l)}{Z_{0-}} & (-1)^n\cos(\beta_{x-}l) \end{pmatrix}^{-1}. \end{aligned} \tag{16}$$

With the above impedance transformation relations at each interface between different chiral layers, we can calculate the input impedance matrix $\overline{Z}_{\text{up}}$ and $\overline{Z}_{\text{dn}}$, looking upward and downward from an arbitrary reference plane as shown in Fig. 2. Using the transverse resonance condition, we can get the dispersion equation for the structure

$$\det[\overline{\boldsymbol{Z}}_{\text{up}} + \overline{\boldsymbol{Z}}_{\text{dn}}] = 0 \tag{17}$$

where det denotes determinant of matrix.

It should be appreciated that the above analysis also holds when some of the materials are achiral, except that a few mathematical expressions need specific attention. When treating achiral media, the field components are expanded in terms of two circularly polarized plane waves with equal wave numbers.

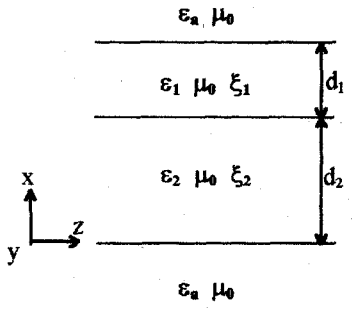

Fig. 4. A two-layer open chirowaveguide.

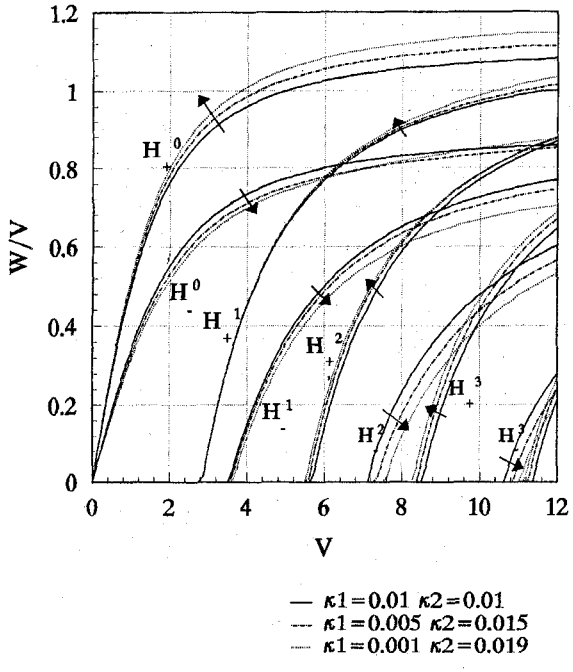

Fig. 5. Dispersion property for the open structure shown in Fig. 4. $v = k_o D\sqrt{\epsilon_1 - \epsilon_a}, w/V = \sqrt{\beta^2 - \epsilon_a}/\sqrt{\epsilon_1 - \epsilon_a}$.

To verify the effectiveness of the network method developed in this paper, we have calculated a two-layer open structure as shown in Fig. 4. The value of media parameter are assigned as

$$\epsilon_1 = \epsilon_2 = 4.41, \quad \epsilon_a = 4.0, \quad \xi_1 = -j2.1\kappa_1,$$
$$\xi_2 = -j2.l\kappa_2, \quad d_1 = D/3, \quad d_2 = 2D/3.$$

When κ_1 and κ_2 are chosen to be equal, we get exactly the same results as in [2]. When κ_1 and κ_2 deviate from the initial value of 0.01 ($\kappa_{2,1} = 0.01 \pm 0.005$, or $\kappa_{2,1} = 0.01 \pm 0.009$), the change of eigenvalue is shown in Fig. 5 by the arrows. Because of $d_2 > d_1$, it is expected that κ_2 contributes more to the change than κ_1 does, i.e. as κ_2 increases, the pairs of curves originally having the same cut off in the chiral limit will more and more separate from each other [2]. This trend can be observed in Fig. 5. Judging from this, the effectiveness and accuracy of the present approach are thus verified, though no comparison is given in Fig. 5 between our results and others because of no data available for a two-layer open chirowaveguide in the literature.

III. Conclusion

This paper presents an equivalent network method for the dispersion analysis of general multilayered planar chirowaveguides. Use has been made of the concepts of multimode network method for planar dielectric waveguides. Different kinds of impedance transformation relations are given, including the transformation of input impedance matrix within a homogeneous layer, the impedance matrix transformation at the interface of two media and the input impedance matrix for a layer terminated with an open or short circuit. Also, the transverse resonance technique is extended to treat the chirowaveguides.

References

[1] H. Cory and I. Rosenhouse, "Electromagnetic wave propagation along a chiral slab," *IEE Proceedings-H*, vol. 138, no. 1, pp. 51–54, Feb. 1991.
[2] M. Oksanen, P. K. Koivisto, and I. V. Lindell, "Dispersion curves and fields for a chiral slab waveguide," *IEE Proceedings-H*, vol. 138, no. 4, pp. 327–334, Aug. 1991.
[3] M. I. Oksanen, J. Hanninen, and S. A. Tretyakov, "Vector circuit method for calculating reflection and transmission of electromagnetic waves in multilayer chiral structures," *IEE Proceedings-H*, vol. 138, no. 6, pp. 513–520, Dec. 1991.
[4] C. R. Paiva and A. M. Barbosa, "A method for the analysis fo bi-isotropic planar waveguides-application to a grounded chiroslab guide," *Electromagn.*, no. 11, pp. 209–221, 1991.
[5] M. I. Oksanen, P. K. Koivisto, and S. A. Tretyakov, "Vector circuit method applied for chiral slab waveguides," *J. Lightwave Technol.*, vol. 10, pp. 2150–2155, Feb. 1992.

Fast and Efficient Extraction of HBT Model Parameters Using Multibias *S*-Parameter Sets

Seonghearn Lee

***Abstract*—Accurate parameter extraction technique has been presented for a small-signal equivalent circuit model of AlGaAs/GaAs HBT's. This technique makes use of multibias data optimization regarding two sets of *S*-parameters in the active mode and one in the cut-off mode, under the physics-based constrain that current-dependent elements in two active bias circuits are linked each other by the ratio of their currents. This multibias optimization as well as the constrain imposed on intrinsic parameters may reduce the degree of freedom of circuit variables and increase the probability of finding a global minimum result. As a result of this extraction, good agreement is seen between the circuit models and their measured *S*-parameters in the frequency range of 0.045 to 26.5 GHz.**

I. Introduction

For the development of microwave circuit applications using heterojunction bipolar transistors (HBT's), it is essential to use an accurate HBT equivalent circuit model for simulating monolithic microwave integrated circuit (MMIC). Although physical and analytical HBT models have been reported previously [1], [2], an empirical HBT model requiring circuit parameters extracted from measurements has been generally used. In order to provide precise parameter values, reliable and efficient extraction method should be established. In a typical approach, a small-signal equivalent circuit model is optimized

Manuscript received June 11, 1995; revised April 19, 1996.
The author is with the Department of Electronic Engineering, Hankuk University of Foreign Studies, Yong-In, Kyung-Gi Do, 449-791, Korea.
Publisher Item Identifier S 0018-9480(96)05647-5.